UNIVERSIDAD DE MÁLAGA

MUCOM Máster Universitario en Simulación Numérica en Ciencia e Ingeniería con COMSOL Multiphysics

TRABAJO FIN DE MÁSTER

Simulación 3D de la distribución espacial de especies químicas asociadas a la corrosión del par Zn-Fe

3D simulation of the spatial distribution of chemical species associated to the corrosion of the Zn-Fe couple

MÁSTER UNIVERSITARIO en

SIMULACIÓN NUMÉRICA EN CIENCIA E INGENIERÍA

con COMSOL MULTIPHYSICS

Autor: António Alexandre da Cunha Bastos

Tutor: Juan Manuel Paz García

Tutor: Emilio Ruiz Reina

21 de junio de 2021

Summary

1. Introduction

This work presents a numerical simulation of the electrochemical processes and associated distribution of chemical species that take place during the corrosion of the zinc-iron galvanic couple. The electrochemical cell analysed in this work was designed for studying the zinc and iron electrodes, isolated or galvanically coupled. In this last case, it provides a clear separation of the anodic and cathodic processes, thus facilitating the investigation of the effects of changes in the environment (including the addition of corrosion inhibitors) towards, not only the overall corrosion process, but also the two partial reactions.

The small size of the cell allows the use of microelectrodes for localised chemical analysis, which is difficult and often impossible with larger cells. For this reason, this work benefited from the existence of many experimental results, namely polarization curves, galvanic current, galvanic potential, potential in solution, current density in solution, pH, and distributions of O_2, Zn^{2+}, Na^+ and Cl^- in solution. This experimental data was used to set the boundary conditions and initial values, and to validate the numerical results.

This document starts with the theoretical foundations of the problem, with a brief description of the importance of the zinc-iron coupling in the corrosion protection of steel, followed by a short overview of the corrosion process, which will help understand the decisions made during the elaboration of the numerical model. Then the model is introduced, with the chosen geometries and meshes, the governing equations, the boundary conditions, initial values, and studies. The model presented here is the most complete and accurate of a series of models that were experimented, including 2D and 3D geometries, and various meshes, physics and boundary conditions. Finally, the results of the numerical simulation are compared with the experimental data in the Results and Discussion section. Finally, the Conclusions and suggestions for Future Work are presented. The document ends with an appendix containing information about the methods and techniques employed in the acquisition of the experimental data presented in this work.

2. Theoretical Foundations

The zinc-iron galvanic coupling is of major importance for the corrosion protection of steel, appearing in galvanised steel and in the cathodic protection with sacrificial zinc anodes of naval ships and offshore structures. To appreciate its importance, it suffices to mention that zinc is the 4th most used metal (after Fe, Al and Cu) and 50% of its amount is used for galvanising steel. When zinc and iron are electrically connected, and both immersed in an aqueous environment, the potential of the couple becomes close to that of zinc, a value where the corrosion of iron is thermodynamically unfavoured.

Corrosion is defined as the spontaneous reaction of a metal (some definitions include all materials) with its environment leading to the modification of the material and/or the environment, usually with negative effects [1]. It has a great impact in our metals-based society. In fact, most studies indicate the direct costs of metallic corrosion to be around 3% of the gross

domestic product (GDP) in each country every year [2]. Indirect costs such as factory shutdown, loss of production, los of efficiency, accidents, image costs and litigations are not included in the sum because they are unpredictable and difficult to account. To understand why corrosion occurs, it is important to note that in the beginning of our Earth, metals were all in the metallic (reduced) state, coming directly from their synthesis in supernovas. They oxidised upon contact with oxidising species in the terrestrial environment, notably O_2, originated after the onset of photosynthesis. The appearance of a O_2 rich atmosphere waited until the metals in the Earth's crust (mainly iron) were oxidized, which took around 10^9 years [3]. Very recently, about 7000 years ago, humankind started using metals, first those in native reduced state (noble or precious metals) and then the others that could be transformed from ore to metal with the help of energy through metallurgical processes. Naturally, in the moment these metals are produced, they become in contact with the atmosphere that kept them in the oxidised form since ever. The natural process by which metals return to their natural oxidized state is corrosion, which can be viewed as the reverse of extractive metallurgy. Corrosion is a thermodynamically favoured process and the energy spent in producing the metals is a direct measure of their tendency to oxidize (return to the native state).

Metallic corrosion is an electrochemical phenomenon involving the oxidation of the metal and reduction of some species from the environment. The overall redox process can be divided in half-reactions, with an anodic half-reaction, the metal oxidation,

$$M(s) \rightarrow M^{n+}(aq) + ne^- \quad (1)$$

and the simultaneous reduction of chemical species in the environment capable of accepting the electrons generated in reaction (1). The most common reactants are water and oxygen, which are omnipresent in the Earth's atmosphere. The main reduction in neutral or alkaline media is,

$$O_2(g) + 2H_2O(l) + 4e^- \rightarrow 4OH^-(aq) \quad (2)$$

and the principal reduction in acidic media is,

$$2H^+(aq) + 2e^- \rightarrow H_2(g) \quad (3)$$

The oxidation and reduction half-reactions take place at the same rate but usually separated in space. The flux of electrons in the metal phase from anodes to cathodes is accompanied in the environment side (solution) by the flow of anions to the anodes and cations to the cathodes, closing the electric circuit. Metal oxidation occurs spontaneously when the equilibrium electrode potential of the metal is more negative than the equilibrium electrode potential of half-reactions (2) and (3). This applies to most metals and is the driving force for their oxidation. The metals that do not naturally corrode have potentials more positive than reactions (2) and (3). Often the rate of corrosion is controlled by the cathodic process. This is because the metal is there ready to oxidize but it depends on the availability of chemical species able to accept the electrons. In ordinary conditions, the oxygen dissolved in water (≈2.3 x 10^{-4} M or 8 mg L^{-1} [4]) determines the corrosion rate but in acidic conditions the concentration of $H^+(aq)$ is much larger and corrosion increases exponentially with the decrease in pH.

After the initial electrochemical half-reactions, the process continues with the chemical reaction of the products of (1)-(3) with the precipitation of corrosion products,

$$M^{n+}(aq) + nOH^{-}(aq) \rightarrow M(OH)_n(s) \quad (4)$$

Many other reactions with chemical species existing in the environment are possible. Common corrosion products include oxides, hydroxides, chlorides, sulphates and carbonates.

This work deals with the corrosion of the zinc-iron couple. The electrochemical responses of zinc and iron corroding alone are sketched in Figure 1 a). The red curves correspond to the half-reactions (1) for Zn and Fe. The solid lines are the oxidation (anodic) branches, and the dashed lines the reduction (cathodic) part of the curves. The dashed cyan line corresponds to the reduction of dissolved O_2 (the linear part is due to the diffusion control of the process, i.e., after a certain overpotential the rate of the reaction no longer depends on the applied potential but on the arrival of the reacting species to the surface). The cyan dotted line corresponds to the water reduction. The blue line is the summation of the two reduction processes. In most cases it is this negative current that dictates the corrosion rate of the metals. Corrosion is a mixed process occurring in a point where the anodic current on the metal meets the cathodic current of the reductions taking place at its surface. A mixed potential is found where the anodic currents match the cathodic currents. This potential is called corrosion potential (E_{corr}) and the matching current is the corrosion current (i_{corr}). The green lines show the experimental curves that would be obtained by polarizing zinc or iron in a linear sweep voltammetry experiment (polarization curve).

When zinc and iron are coupled together the corrosion process is dominated by the metal with more negative potential, zinc, which will oxidize and shift the potential of the other metal (iron in this case) to a region where the tendency is for its reduction (if Fe^{2+} would be available it could be reduced at the surface of Fe). Iron will therefore be a cathode and reactions (2) and (3) will take place on its surface, forcing an extra oxidation of zinc to "feed" this additional reduction. Note that the reductions still can take place on zinc. A sketch of this process is presented in Figure 1 b). The increase in the cathodic current is due to the duplication of the electrode area where the reductions take place (in fact, this current is proportional to the actual area of the couple with respect to the initial zinc area but also depends on the reactivity of the surface towards the reduction reactions). The potential of the zinc electrode will shift to a new more positive value, the one where the anodic current matches the new negative current in play.

Figure 2 shows the electrochemical cell studied in this work. The reactions are taking place in each electrode, as just discussed, and it is possible to measure many quantities involved in the process, like the corrosion potential of the galvanic couple (E_{galv}), the galvanic current flowing between the two electrodes (I_{galv}) and polarization curves of the uncoupled and coupled electrodes. It was also possible to measure the potential and the current density in solution, as well as the pH, and local concentrations of O_2, Zn^{2+}, Na^{+} and Cl^{-}. The mapped regions are shown in Figure 2 b) with maps normal and parallel to the surface. The experimental details are presented in Appendix 1, and the results will be presented in the Results and Discussion section.

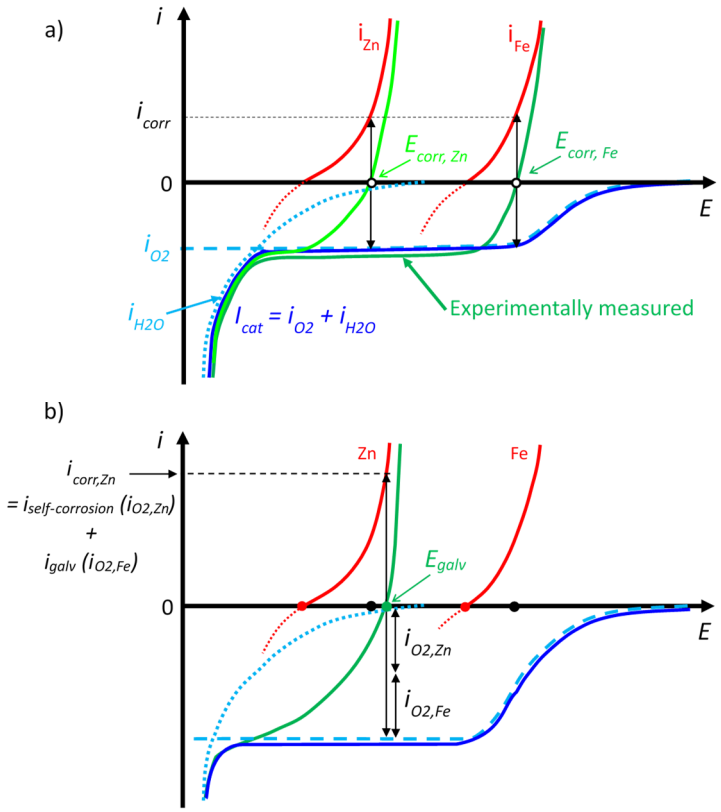

Figure 1 – Sketches with the partial (red and blue) and complete (green) polarization curves of zinc and iron electrodes a) corroding alone and b) galvanically coupled.

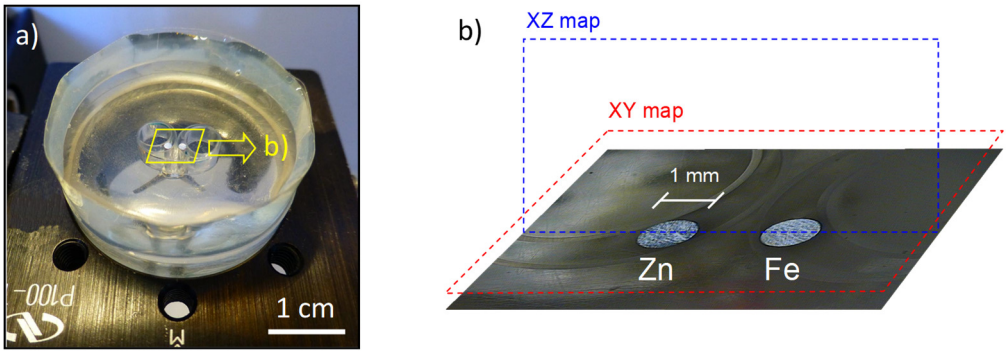

Figure 2 – a) Zn-Fe electrochemical cell and b) position of the scanned areas with microelectrodes.

Figure 3 presents sketches with chemical and electrical interpretations of the process occurring in the electrochemical cell. The objective of this work is to go beyond these sketches and be able to numerically simulate the corrosion process and replicate the existing experimental results. This would enable further analysis on the effects of changing parameters such as the geometry of the cell, solution composition, different electrode materials, etc.

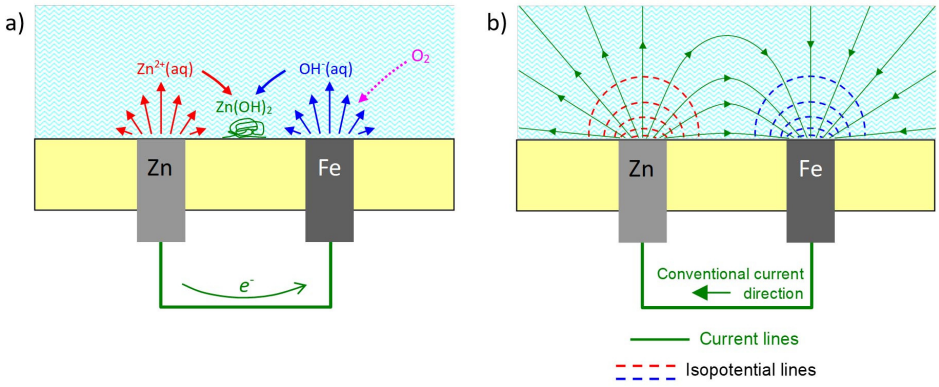

Figure 3– a) Chemical interpretation and b) electric interpretation, of the processes occurring in the galvanic cell.

3. Geometry

Figure 4 a) shows the galvanic cell and Figure 4 b) presents the geometry used to solve the problem, corresponding to half of the cell geometry, for saving computing time. The height is the solution layer thickness. The geometry was parametrized to facilitate the change of the cell dimensions and for parametric studies. The boundaries of interest are: 1 (zinc electrode, anode), 2 (iron electrode, cathode), 3 (top, solution/air interface), 4 (symmetry plane), 5 (side walls), and 6 (epoxy mount surface). The rectangle in the symmetry plane has the same size of most of the maps and is there to facilitate the demonstration of results.

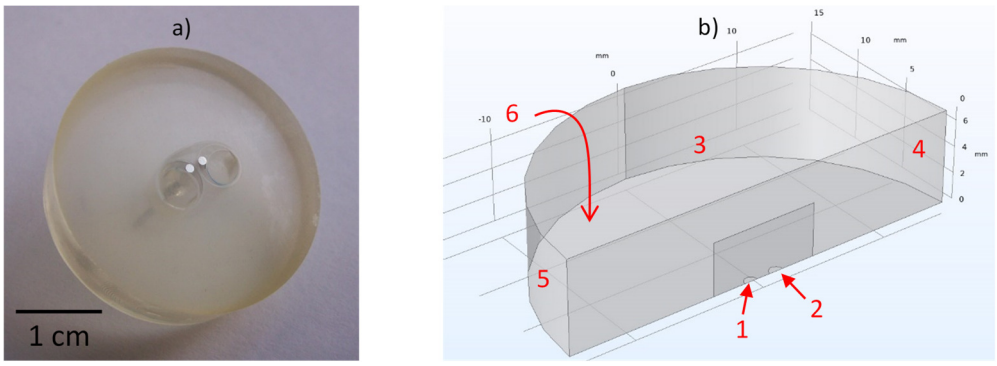

Figure 4 – a) Zn-Fe galvanic couple and b) the geometry used to model the problem.

4. Mesh

The computational domain was discretised using the two meshes presented in Figure 5. In both a mesh refinement was made close to the electrodes, where the concentrations and potential gradients are expected to be the highest. The simpler mesh was used for calibrating the model and obtain results in a shorter time. The final results were obtained with the denser mesh. A finer discretization did not improve the solution accuracy but significantly extended the computing time.

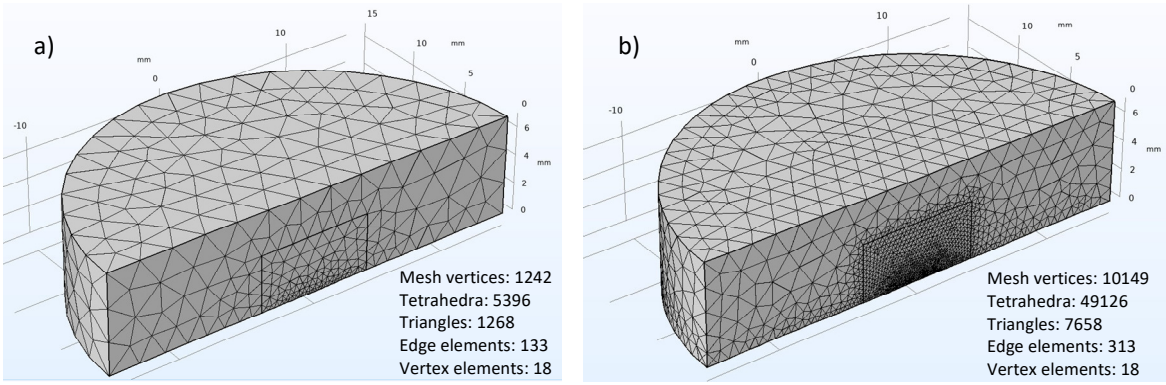

Figure 5 – The two meshes used in the simulations.

5. Materials

Zinc and iron were selected as materials for this model. Presently they are needed only for providing the experimental polarization curves as input information (boundary conditions) of the electrochemical kinetics of anode and cathode. If the model used other parameters, like Tafel parameters, the materials assignment would be unnecessary.

6. Equations and Physical Interfaces

The model was set in COMSOL Multiphysics 5.6. using the *Tertiary Current Distribution, Nernst-Plank Interface* with the *water-based with electroneutrality* charge conservation model.

The governing equations of this model are the mass balances of each species i,

$$\frac{\partial c_i}{\partial t} = -\nabla \cdot J_i + R_i \tag{5}$$

where c_i (mol m^{-3}) is the concentration of species i, J_i (mol m^{-2} s^{-1}) is the molar flux of species i and R_i is the source term of species i, accounting for its production/consumption rate in homogeneous reactions in solution. The other governing equation warrants electroneutrality,

$$\sum_i^n z_i\, c_i = 0 \tag{6}$$

with z_i being the charge of species i. The electroneutrality was maintained by the species of the water ionization, H^+ and OH^-.

The molar flux J_i obeys the Nernst-Plank equation and is the sum of contributions from diffusion, migration and convection,

$$J_i = -D_i\, \nabla c_i - z_i u_i F c_i \nabla \phi + c_i \vartheta \tag{7}$$

with D_i and z_i, respectively, the diffusion coefficient ($m^2\ s^{-1}$) and charge of species i, u_i the ionic mobility of ion i, F the Faraday constant (96485 C mol^{-1}), ϕ the solution potential and ϑ the solvent velocity ($m\ s^{-1}$). The ionic mobility is given by,

$$u_i = \frac{D_i}{RT} \tag{8}$$

where R is the universal gas constant (8.314 J $mol^{-1}\ K^{-1}$) and T is the temperature (298.15 K). The cell is quiescent; therefore, the solvent velocity is assumed to be $\vartheta = 0$. For the moment, the natural convection is not included in the model [5-7].

The chemical species under consideration are presented in Table 1, together with some of their parameters.

Table 1 – Species considered in the simulation.

Species	c_i^0 (mol m^{-3})	z_i	D_i (x10^9 $m^2\ s^{-1}$)
O_2	0.23	0	1.96 [8]
Na^+	5	+1	1.23 [8]
Cl^-	5	-1	1.19 [8]
H^+	-	+1	9.31 [8]
OH^-	-	-1	5.26 [8]
Fe^{2+}	10^{-3}	+2	0.65 [8]
Zn^{2+}	10^{-3}	+2	0.7 [8]

7. Boundary conditions

Boundaries 1 and 2 (see Figure 4) correspond to the zinc and iron electrodes, respectively. Equation (1) takes place on zinc (M = Zn, n = 2) and equation (2) occurs on iron. It is possible that (2) also occurs on zinc and iron oxidizes on boundary 2. This kinetic information can be set in COMSOL in different ways. In this work two were experimented: i) Tafel parameters from the literature and ii) experimental polarization curves.

The anodic Tafel equation for the oxidation of zinc is,

$$i_{Zn} = i_{0,Zn}\ 10^{\frac{\eta}{A_{Zn}}} \tag{9}$$

where $i_{0,Zn}$ is the exchange current density, A_{Zn} is the Tafel slope, and η is the overpotential, defined as,

$$\eta = \phi_s - \phi_l - E_{eq} \tag{10}$$

where ϕ_s is the potential in the electrode (metal), ϕ_l is the potential in solution (liquid) and E_{eq} is the equilibrium potential of the electrochemical reaction.

A similar equation was used for the oxidation of iron.

The oxygen reduction, equation (2), taking place in each electrode was described by the following cathodic Tafel equation,

$$i_{O_2,Tafel} = -i_{0,O_2}\, 10^{\left(\frac{\eta}{A_{O_2}}\right)} \quad (11)$$

It was further considered that the oxygen reduction reaction was dominated by the diffusion of dissolved O_2 from the bulk of the solution to the electrodes surfaces and the following equation was included,

$$i_{O_2} = \frac{i_{O_2,Tafel}}{1 + \left|\frac{i_{O_2,Tafel}}{i_{lim}}\right|} \quad (12)$$

where i_{lim}, is the limiting current.

The parameters used in the model are presented in Table 2 and were taken from the literature.

Table 2 – Electrochemical parameters considered in the model.

Parameter	Value	Reference
E_{Zn}^0	-1.004 V_{SCE}	[9]
$i_{0,Zn}$	0.1 A m^{-2}; 4.48 A m^{-2}	[9-10]
A_{Zn}	22 mV, 28±3 mV	[9-12]
E_{Fe}^0	-0.681 V_{SCE}	[9]
$i_{0,Fe}$	0.28 A m^{-2}	[9-10]
A_{Fe}	0.154 V	[9-10]
E_{O2}^0	0.650 V_{SCE}	[9]
$i_{0,O2\ on\ Zn}$	0.888 x 10^{-4} A m^{-2}	[9-10]
$A_{O2,\ on\ Zn}$	-0.055 V	[9-10]
$i_{0,O2\ on\ Fe}$	0.888 A m^{-2}	[9-10]
$A_{O2,\ on\ Fe}$	-0.055 V	[9-10]
$i_{lim,O2}$	0.2 – 0.5 A m^{-2}	[11]

V_{SCE} = V vs SCE (saturated calomel electrode)

In the model that is shown in this work, the current density expression in each electrode was set by experimental polarization curves, added as interpolation functions in the material (Zn and Fe) nodes. The experimental curves are presented in Figure A2 (1 hour of immersion).

The top boundary (boundary 3 in Figure 4) is the solution-air interface and allows the normal flux of oxygen, F_{O_2}, given by

$$F_{O_2} = \frac{\partial c_{O_2}}{\partial n} = F_{O_2,max}\left(1 - \frac{c_{O_2}}{c_{O_2}^{sat}}\right) \quad (13)$$

where c_{O_2} is the local concentration of O_2, $c_{O_2}^{sat}$ is the solubility of O_2 in solution and $F_{O_2,max}$ is the maximum dissolution rate of O_2 at 25 ºC (2.6-4.5 x 10^{-5} mol m^2 s^{-1} [13]). An average value of $F_{O_2,max}$= 3.5 x 10^{-5} mol m^2 s^{-1} was be used in the simulations The solubility of O_2 depends on

temperature, pressure, but also on the concentration of NaCl [14],

$$c_{O_2}^{sat}(mol\ m^{-3}) = 0.23\ e^{\left(-3.63\times10^{-4}\times c_{Cl^-}\right)} \quad (14)$$

$c_{O_2}^{sat}$ has been introduced in the model as a variable. The use of a non-constant concentration of O_2 can be important when using different concentrations of NaCl and in future simulations when solution evaporation will be considered. In this model, the same simulation results were obtained if, instead of F_{O_2}, a *Concentration* boundary condition was set in boundary 3 with c_{O2} = 0.23 mol m^{-3}. Such a Concentration boundary condition was established for the chemical species in the model using the values presented in Table 1.

The same values in Table 1 were also set as Initial Values. A solution potential of $-E_{Zn}^{0}$ (-Eeq_Zn) was also set as an initial value.

The walls and the epoxy base (boundaries 5) were assumed to be insulating walls, with the normal fluxes of species and the current in solution (i_l), all set to zero,

$$-\boldsymbol{n}\cdot J_i = 0 \quad , \quad -\boldsymbol{n}\cdot i_l = 0 \quad (15)$$

Finally, a Symmetry boundary condition was assigned to boundary 4, with no flux properties.

8. Studies

The simulation was made with a *Time dependent* study, for different output times: 1 µs, 1 ms, 1s, 1 h and 1 day. Only the times for 1 hour and 1 day are important but it was decided to try shorter times as well. In some parallel studies the simulation run also for the first day of immersion with intervals of 1 hour, and 10 days period with intervals of 1 day.

9. Results and Discussion

As stated above, the objective of this work is to simulate the corrosion of a model Zn-Fe galvanic couple and compare the numerically simulated results with those obtained experimentally. Since there are many results due to the great number of parameters of interest, and for the sake of a clearer presentation, a first comparison is made between the results obtained with the two meshes and the two input electrochemical parameters (polarization curves and Tafel equation). The comparison is based on the calculated values of E_{couple}, the corrosion potential of the couple, I_{galv}, the galvanic current flowing between Zn and Fe, and ΔE, the potential difference in solution close to the electrodes with respect to the mean value in the bulk of the solution. Afterwards, the maps with the distribution of chemical species in solution obtained experimentally and resulting from numerical simulation will be compared. For saving space, only maps in the normal direction to the cell surface (XZ plane) will be presented.

Starting with the comparison of the influence of the mesh and of the input electrochemical parameters, Table 3 clearly shows a minor effect of the mesh in the computed values. The importance of the mesh becomes evident when comparing the maps of chemical distribution, with smoother contours for the simulations with the finer mesh. More important is the

influence of the electrochemical input parameters. Using polarisation curves, a I_{galv} closer to the experimental data was obtained. Conversely, the closest E_{couple} was found using Tafel equation parameters from the literature. Regarding the potential in solution, ΔE, the simulation with polarisation curves gives an overestimation of the measured values while the simulation with Tafel equation gives an underestimation. It is important to note that the experimental map (Figure 6 a)) did not reach the surface, therefore the highest potential difference was not registered, which means that the values from the simulation using polarization curves are more accurate. For this reason, and also due to the lower computing time, most of the simulations were conducted with this model.

Table 3 – E_{couple}, I_{galv} and ΔE in solution, from experiments and from numerical modelling.

	Experimental	Polarization curves		Tafel equation	
		Mesh1	Mesh2	Mesh1	Mesh2
E_{couple} (V_{SCE})*	-1.015	-0.934	-0.934	-1.005	-1.007
I_{galv} (10^{-7} A)	7.5	7.15	7.15	1.86	1.96
ΔE (mV)	12	17	17	7	7
Computing time		1 min 40 s	34 min 34 s	2 min 54 s	1 h 43 min 48 s

*Saturated calomel electrode

It is also informative to look to the evolution of the same parameters calculated for different times. It is likely that times less than 1 second have no real physical meaning in the system under study, and even in the first minutes after the galvanic coupling, the system can be unstable, so that only the calculations for 1 hour and 1 day are trustful. In any case, Table 4 shows that the values are not that very different, with no changes up to 1 ms and then rapidly evolving to the values calculated for 1 day of immersion. Simulations were made for every hour during the first 24 hours of immersion. Very small variations could be detected for the first 2-4 hours, but then the system was stable with no change in the parameters. Another study calculated the values up to 10 days, and no changes were verified compared to the values found for 1 day of immersion.

Table 4 – E_{couple}, I_{galv} and ΔE with time according to a study based on Mesh2 and polarization curves.

Time	Ecouple (V_{SCE})	Igalv (10^{-7} A)	ΔE (mV)
1 µs	-0.9310	6.9967	24
1 ms	-0.9310	6.9965	24
1s	-0.9315	6.9625	23
1 h	-0.9335	7.1208	18
1 d	-0.9340	7.1525	17

Finally, it is worth mention the effect of increasing the concentration of NaCl. The computed values are presented in Table 5 and indicate that, as the solution becomes more conductive, E_{couple} becomes slightly more negative, I_{galv} slightly increases, and ΔE practically vanishes. This potential in solution is the ohmic drop related to the transport of (ionic) current in solution. Following Ohm's law, since the conductivity increases, and I_{galv} is practically the same, the potential must decrease.

Table 5 – E_{couple}, I_{galv} and ΔE with different concentrations of NaCl.

[NaCl] / M	Ecouple (V_{SCE})	Igalv (10^{-7} A)	ΔE (mV)
0.005	-0.934	7.15	17
0.05	-0.939	7.56	3
0.5	-0.940	7.63	0.3

The next sections show the experimental and simulated maps of several quantities in solution above the Zn-Fe couple: potential, current density, O_2, pH, Zn^{2+}, Na^+ and Cl^-. The simulations were made with the model with polarisation curves and the finer mesh, Mesh2.

9.1. Potential in solution

Figure 6 shows the experimental and the simulated potential in solution established during the corrosion of the Zn-Fe galvanic corrosion. This potential is related to the ionic current flowing in the cell, transported by all charged species in solution. The values are not very different, from -6 mV to 6 mV in the experimental map and 8.6 mV to -8.8 mV in the simulation. One reason for the difference is that the experimental map started 50 µm above the surface (to avoid breaking the glass microelectrode) missing the region of higher potential difference, which is in the vicinity of the electrodes' surfaces. The major potential changes occur close to the electrodes due to the concentration of current lines in those locations. The main difference between the maps is the point of zero potential. It is placed in the middle of the experimental map, while in the simulation most of the potential drop occurs in the vicinity of the anode (Zn).

9.2. Current density in solution

The local current density in solution was measured with a Scanning Vibrating Electrode Techmique (SVET), equipment that can measure two components of the current density vector. Figure 7 shows just the z component. The calculated values seem to be similar to the experimental values, taking into account that the SVET probe approached the surface just down to 100 µm, missing the region of higher currents. For a more accurate comparison it is possible to present the simulated values coincident with the region of the cell that was actually mapped.

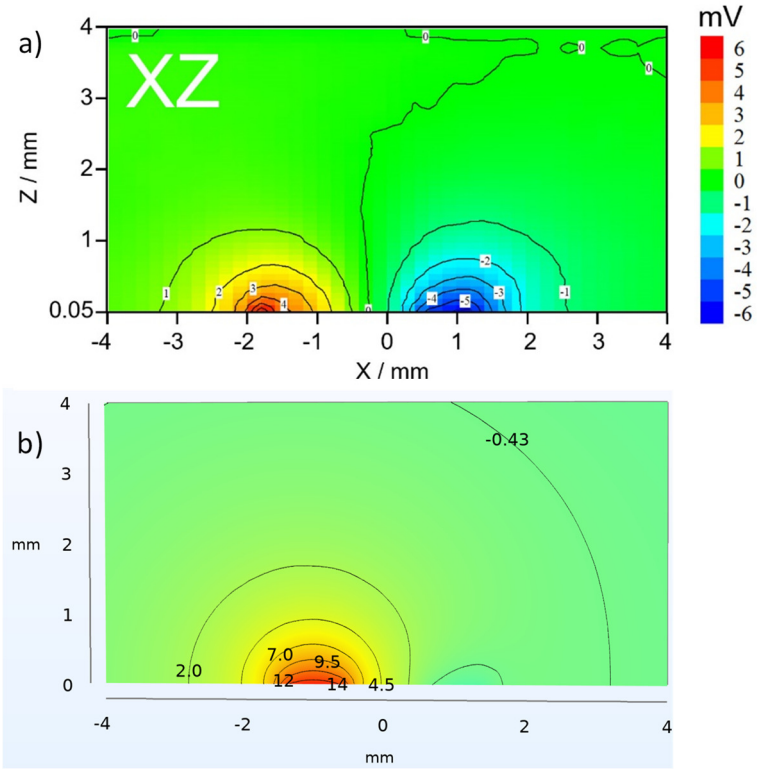

Figure 6 – a) experimental results and b) numerical simulation, of the potential in solution (0.005 M NaCl) during the galvanic corrosion of the Zn-Fe couple.

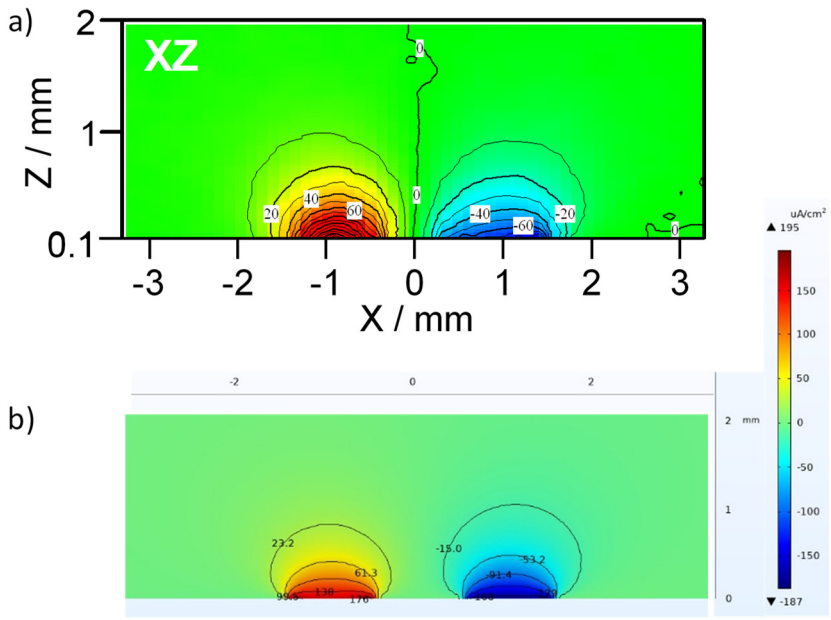

Figure 7 – a) experimental results and b) numerical simulation, of the current density in solution (0.005 M NaCl) during the galvanic corrosion of the Zn-Fe couple.

9.3. Distribution of O_2

The distribution of dissolved oxygen in solution is presented in Figure 8. The experimental values are 50% lower than the expected. This is attributed to the partial blocking (fouling) of the microelectrode tip during the measurement, by the precipitation of impurities and contaminants, including $Zn(OH)_2$ from the Zn^{2+} ions in solution. The measurement started from the top and continued until reaching a level 50 µm above the surface. It is noticeable a small decrease in current from the upper to the lower part of the map. Despite these shortcomings, it is clear a depletion of O_2 near the cathode owing to its consumption in reaction (2). The simulation shows a map with the same depletion of O_2, but with a round shape in contrast with the depressed shape observed in the experimental map. This, as will be seen it the following maps, is due to the neglect of the effect of natural convection which forces the diffusion layer to exist only in a region close to the electrode surface. The account of natural convection must be made explicitly, and this is the first improvement to be made to this model. Quite strange is the region of negative concentration of O_2 just above the cathode. This certainly comes from a numerical problem due to the fact that no information was given to the model about O_2 being the limiting reactant of the corrosion process.

9.4. pH variation in solution

The pH in solution increases near the cathode, resulting from reaction (2), which consumes O_2 and produces OH^-. The maximum measured pH is about 1 pH unit lower than the simulation. A few reasons can be advanced for the discrepancy. Experimentally, the microelectrode did not touch the cathode's surface. To avoid damaging the microelectrode, the measurement stopped 10-20 µm above the surface, precisely the position of highest pH. From the simulation part, there are a few processes not yet considered in the model that can decrease the local pH, namely the consumption of OH^- by reaction with Zn^{2+} to produce $Zn(OH)^-(aq)$, $Zn(OH)_2(aq)$, $Zn(OH)_2(s)$,etc, and the mixing effect of the natural convection.

It is easily perceptible in the experimental map that the pH is fairly constant in most of the volume of the solution increasing only at distances closer than 0.5 -1 mm to the cathode. This has been observed with O_2 and will be seen in the following maps of the other chemical species.

The experimental map also reveals a small acidification near the anode, explained by the local hydrolysis of Zn^{2+} ions,

$$Zn^{2+}(aq) + H_2O(l) \rightarrow Zn(OH)^+(aq) + H^+(aq) \qquad (16)$$

It is expected that after the homogeneous reactions are included in the model, the simulations will be able to predict it.

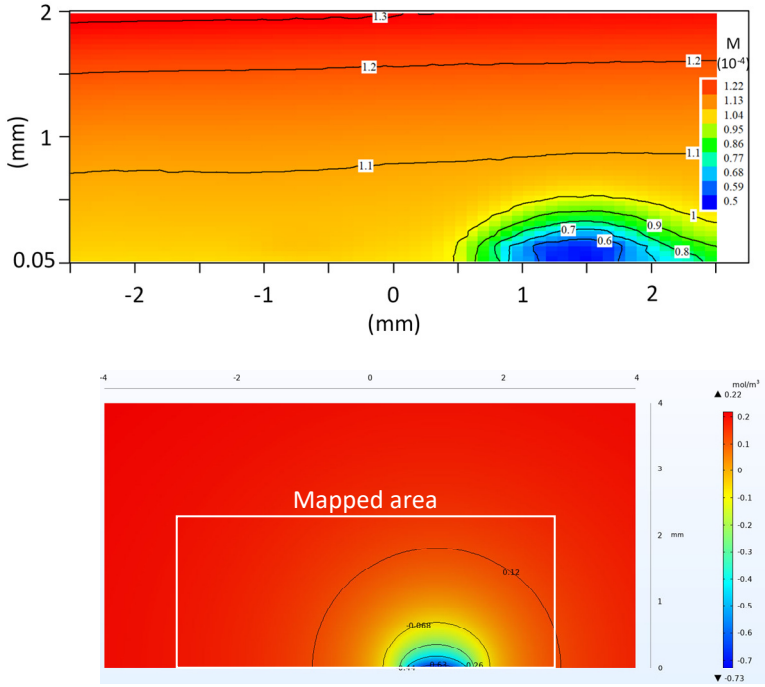

Figure 8 – a) experimental results and b) numerical simulation, of the distribution of dissolved O_2 in solution during the galvanic corrosion of the Zn-Fe couple.

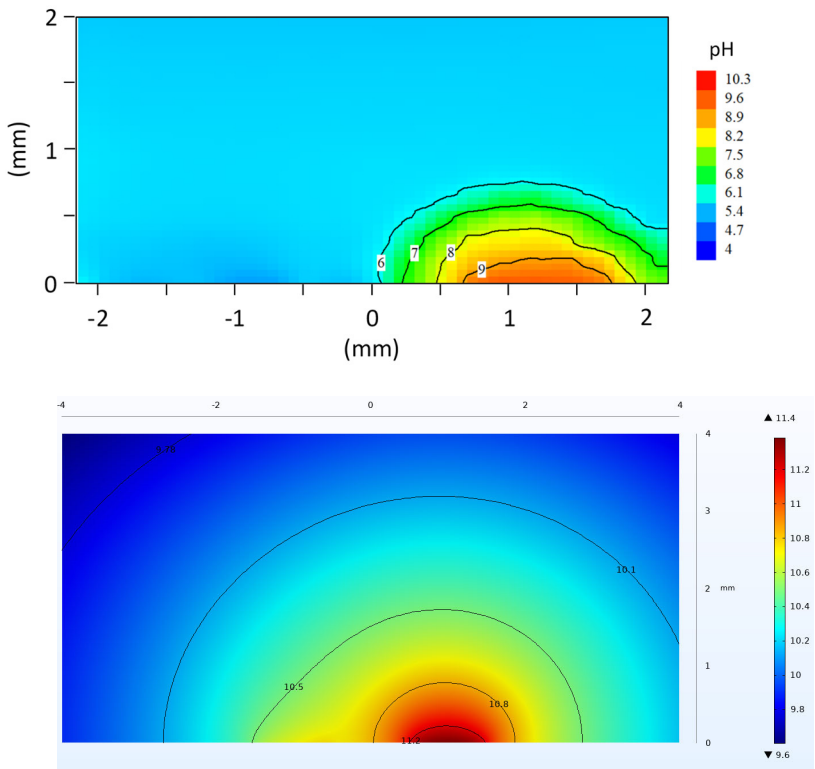

Figure 9 – a) experimental results and b) numerical simulation, of the solution pH during the galvanic corrosion of the Zn-Fe couple.

9.5. Distribution of Zn^{2+}

Figure 10 shows the experimental and the numerical simulation of the distribution of Zn^{2+} ions in solution. It is important to stress that the units of the two maps are not the same. The experimental map shows pZn (-log a_{Zn}) while the simulation map shows concentration (mol m^{-3}). Naturally, it would have been better to show the two maps with the same units. A higher pZn corresponds to a lower concentration and vice-versa. In any case, what is important to remark is the similarity in values close to the electrode. The maximum value in the simulation plot is 3.76 mM which corresponds to pZn=2.4. The simulation map shows the diffusion of Zn^{2+} from the anode to the volume of solution without any zinc ions. The experimental map is more complex, with the same diffusion from the source (the oxidizing zinc electrode) but also a bulk solution with zinc ions and a region close to the cathode without Zn^{2+}. It is possible to explain these features: the bulk value comes from zinc ions being accumulated in solution from the beginning of immersion until the moment of measurement, and the region of depletion near Fe is the result of the reaction with OH^- to produce $Zn(OH)_n^{(2-n)}$ species. There is an alternative explanation. The bulk value is due to the response of the electrode to interfering ions, giving signal even in the absence of Zn^{2+}. The calibration plot of the Zn-selective microelectrode shown in Figure A5 strongly points to this hypothesis. Further, if Zn^{2+} is inexistent in solution, then how to explain its depletion near the cathode? The reason can be also due to the microelectrode response. It might have some sensitivity to pH or even to the potential in solution (a fact often disregarded in potentiometry simply because the measurements are typically performed in a beaker without electric currents flowing therein). Such a potential change would be interpreted in the calibration curve as a decrease of Zn^{2+}. it is an interesting aspect for further investigation.

9.6. Distribution of Na^+ and Cl^-

Na^+ and Cl^- ions will move in solution to compensate the excess of charge being produced at the electrodes. The cation (Na^+) migrates to the cathode (to compensate the excess of OH^-) and will sense a repulsion from the anode. The anion (Cl^-) will migrate to the anode (to compensate the excess of Zn^{2+}) and will be "repelled" by the cathode. This can be seen in Figure 11 with the map of Na^+. The case of chloride ions, presented in Figure 12, shows the opposite of what has been written. This unexpected behaviour might be due to an abnormal response of the chloride ion selective microelectrode: it might be responsive to pH as to chloride and, when approaching the Fe electrode, the increasing in pH shifts the potential to more negative values, being interpreted in the calibration curve as an increase of chloride. The response of the electrode to pH can be easily tested. If confirmed a different electrode must be used.

One final word about the simulations with different concentrations of NaCl. No changes were observed in the chemical composition maps except for Na^+ and Cl^-. Since the corrosion rate is determined by the amount of O_2, the NaCl concentration only plays a role in the conductivity of the solution. Given that the current flowing in solution was practically the same, the amount of Na^+ and Cl^- transported was the same in 5, 50 or 500 mM NaCl. However, the concentrations increased 10 and 100 times, and the actual changes, being nominally the same, were comparatively less important in the higher concentrated solutions.

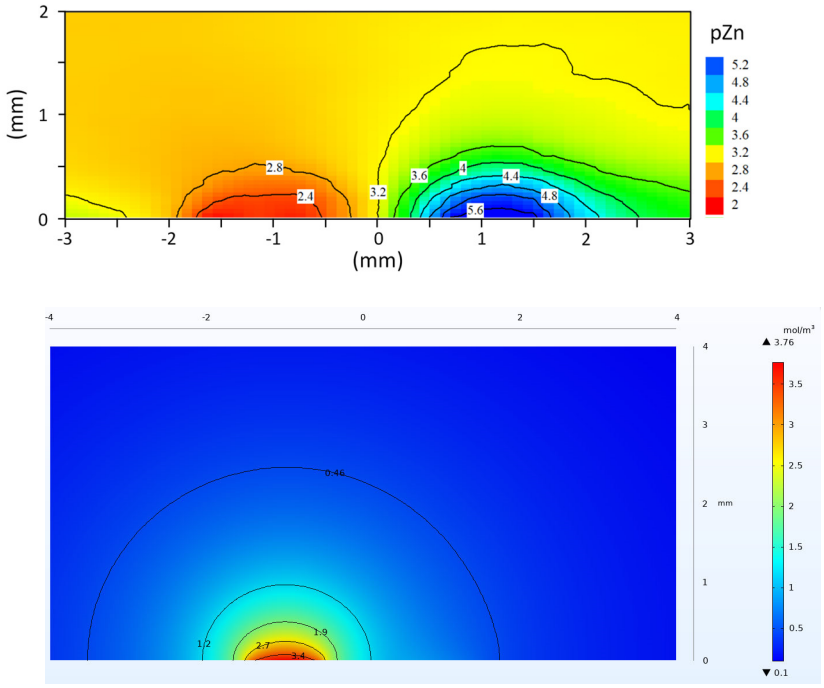

Figure 10 – a) experimental results and b) numerical simulation, of the distribution of Zn^{2+} in solution during the galvanic corrosion of the Zn-Fe couple.

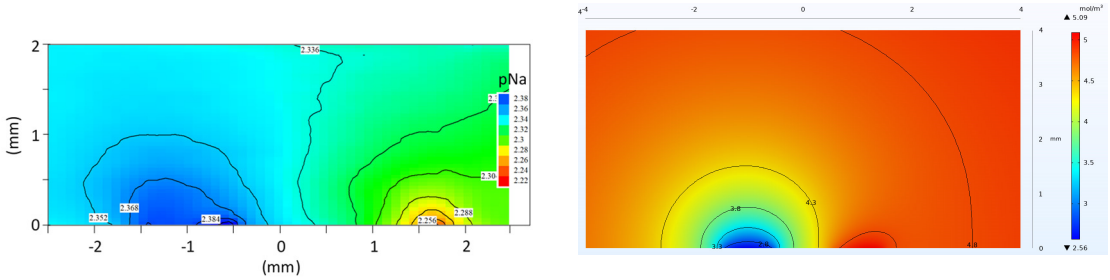

Figure 11 – a) experimental results and b) numerical simulation, of the distribution of Na^{+} in 0.005 M NaCl solution during the galvanic corrosion of the Zn-Fe couple.

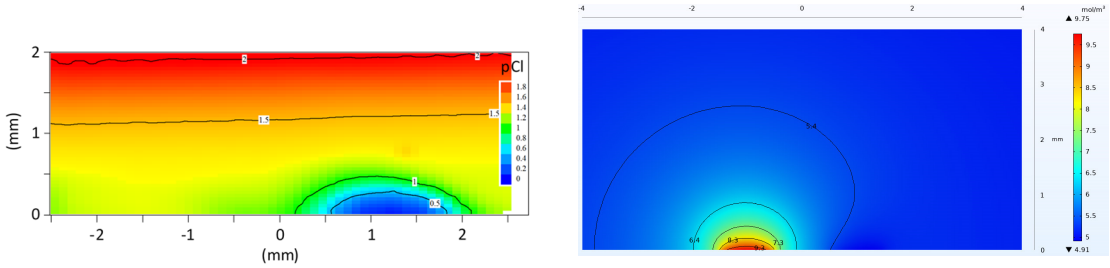

Figure 12 – a) experimental results and b) numerical simulation, of the distribution of Cl^{-} in 0.005 M NaCl solution during the galvanic corrosion of the Zn-Fe couple.

10. Conclusions

The objective of this work was to numerically simulate the corrosion of a model Zn-Fe electrochemical cell, replicating existing experimental results.

A model was developed capable of replicating most of the experimental observations.

The main problem was the lack of natural convection, with the consequent development of a diffusion layer extending to the entirety of the model volume. Divergences were observed in the maps for Zn^{2+} and Cl^{-} but it is possible that the reason lies on the microelectrodes used for the measurements. Selectivity tests will be performed to confirm this hypothesis. More difficult to solve is the appearance of a negative concentration in some of the maps of O_2, particularly in the cases with higher current densities.

The influence of the type of mesh and input electrochemical parameters was investigated.

Significant improvements are expected when the model includes natural convection and homogenous chemical (precipitation) reactions. Once set, this model can be easily modified for studying the effect of geometry parameters (distance between electrodes, electrodes sizes, thickness of solution layer), the nature of the electrodes and type of electrolyte species.

11. Future work

Future work is planned for improving the model by i) adding natural convection, ii) include precipitation reactions and iii) consider the possibility of solution evaporation.

i) Natural convection.

In the absence of convection, the simulated diffusion layer extends to all the computational domain which is not realistic. It is well known, and the present results also show it, that a diffusion layer exists close to the electrodes, the rest being the bulk of the solution, with constant chemical composition. The reason is the existence of a natural convection arising from local temperature and density gradients, vibrations, evaporation, etc, which lead to microscopic motion of the fluid and the mixing of the solution except in the regions close to the electrodes where reactions are taking place. This concept was introduced by Levich [5]. Based on this work Amatore [6] introduced the concept of micro-convection and showed that it can be described by a diffusion-like term, $-D_{\mu\mathrm{conv}}\,\nabla c$. The concept was later extended to multi-ion systems [7]. Equation (7) can be written with the micro-convection term,

$$J_i = -\left(D_i + D_{\mu conv}^{ref}\right)\nabla c_i - z_i u_i F c_i \nabla\phi \qquad (17)$$

The term $D_{\mu\mathrm{conv}}^{\mathrm{ref}}$ is independent of species i depending only on the distance to the electrode d,

$$D_{\mu conv}^{ref} = 1.5072 \cdot D^{ref} \left(\frac{d}{\delta^{ref}}\right)^4 \quad (18)$$

where D^{ref} is a constant with units of diffusion coefficient and δ^{ref} is a distance scaling parameter. According to this equation, when the distance to the electrode is larger than δ^{ref}, the micro-convection becomes dominant. Oxygen has been taken as the reference species because $\delta_{O_2}^{\mathrm{ref}}$ can be estimated from experimental data. This approach used a numerical approximation to mimic the effect of flow, without actually solving it. It is worth mention alternative ways to overcome this problem: one is to solve an often-unknown fluid flow [15,16], the other is to make an artificial separation of the electrolyte into diffusion layer and bulk solution [17].

ii) Precipitation reactions.

With the release of Zn^{2+} and OH^- ions into solution there will be a moment where these ions meet and homogeneous chemical reactions will take place, ultimately leading to their precipitation in the form of corrosion products. Table 6 shows a few of the possible reactions to occur that the model will take into consideration.

Table 6 – Homogeneous chemical reactions to be considered in the simulation.

Reaction	log(K) at 25ºC	Reference
$Zn^{2+} + OH^- \Leftrightarrow Zn(OH)^+$	5.05	[18]
$Zn(OH)^+ + OH^- \Leftrightarrow Zn(OH)_2(aq)$	6.06	[18]
$Zn(OH)^+ + OH^- \Leftrightarrow Zn(OH)_2(s)$	3.0	[18]
$Zn(OH)_2(aq) \Leftrightarrow Zn(OH)_3^-$	2.5	[18]

For longer immersion times, the presence of CO_2 and the formation of carbonates must also be considered. The precipitation reactions can be solved in the model [9,19-20] or be analysed in the post-processing [10].

iii) Solution evaporation.

Solution evaporation can be a common problem, being worth modelling. This can be done with a moving mesh [9,19-20]. Water will evaporate but all other chemical species will remain, and their concentration will increase. As the solution becomes more concentrated the diffusion coefficients will decrease. A semi-empirical model based on equation,

$$D_i = D_i^0 \, e^{(-a_i \cdot c_{Cl^-})} \quad (19)$$

has been developed by Lohrengel *et al.* [21] and used with success by Van Damme *et al.* [22] and Simillion *et al.* [9] in concentrated solutions. D_i^0 is the diffusion coefficient at infinite dilution and a^i is a fitting parameter that depends on the species. The oxygen solubility will also decrease but this is already considered in equation (14).

References

[1] ISO 8044:2020 - Corrosion of metals and alloys - Vocabulary., International Sandardisation Organisation, 2020.

[2] J. Kruger., "Cost of Metallic Corrosion," in *Uhlig's Corrosion Handbook 3rd Edition*, R. W. Revie (Editor), John Wiley & Sons Inc, 2011, pp. 10–15.

[3] H.D. Holland, The oxygenation of the atmosphere and oceans, Phil. Trans. R. Soc. B 361 (2006) 903.

[4] M. Geng, Z. Duan, Prediction of oxygen solubility in pure water and brines upto high temperatures and pressures, Geochim. Cosmochim. Acta 74 (2010) 5631.

[5] V. Levich, Physicochemical Hydrodynamics, Prentice-Hall, Englewood Cliffs,NJ, 1962.

[6] C. Amatore, S. Szunerits, L. Thouin, J.-S. Warkocz, The real meaning of Nernst's steady diffusion layer concept under non-forced hydrodynamic conditions. A simple model based on Levich's seminal view of convection's steady diffusion layer concept under non-forced hydrodynamic conditions, J. Electroanal. Chem. 500 (1-2)(2001) 62.

[7] O. Dolgikh, A. Demeter, A.C. Bastos, V. Topa, J. Deconinck, A practical way to model convection in non-agitated electrolytes, Electrochem. Commun. 37(2013) 20.

[8] CRC Handbook of Chemistry and Physics 85th Ed., D.R. Lide (Editor), CRC Press, Boca Raton, 2005.

[9] M. Saeedikhani, N. Van den Steen, S. Wijesinghe, S. Vafakhah H. Terryn, D.J. Blackwood, Moving Boundary Simulation of Iron-Zinc Sacrificial Corrosion under Dynamic Electrolyte Thickness Based on Real-Time Monitoring Data, J. Electrochem. Soc. 167 (2020) 041503.

[10] F. Thébault, B. Vuillemin, R. Oltra, C. Allely, and K. Ogle, Protective mechanisms occurring on zinc coated steel cut-edges in immersion conditions, Electrochim. Acta 56 (2011) 8347.

[11] M. Attarchi, A. Brenna, M. Ormellese, FEM simulation of corrosion under macro-cell mechanism, Corros. Sci. 179 (2021) 109116.

[12] X.G. Zhang, E.M. Valeriote, Galvanic protection of steel and galvanic corrosion of zinc under thin layer electrolytes, Corros. Sci. 34 (1993) 1957.

[13] H. Davis, G. Crandall, The role of the liquid stationary film in batch absorptions of gases. I. Absorption's involving no irreversible chemical reactions, J. Am. Chem. Soc. 52 (1930) 3757.

[14] F.J. Millero, F. Huang, A.L. Laferiere, Solubility of oxygen in the major sea salts as a function of concentration and temperature, Marine Chem. 78 (4) (2002) 217–230.

[15] V. Topa, A. Demeter, L. Hotoiu, D. Deconinck, J. Deconinck, A transient multi-ion transport model for galvanized steel corrosion protection, Electrochim. Acta 77 (2012) 339.

[16] D. Deconinck, S. Van Damme, J. Deconinck, A temperature dependent multi-ion model for time accurate numerical simulation of the electrochemical machining process., Part II: Numerical simulation, Electrochim. Acta 69 (2012) 120.

[17] F. Thebault, B. Vuillemin, R. Oltra, C. Allely, K. Ogle, Reliability of numerical models for simulating galvanic corrosion processes, Electrochim. Acta 82 (2012) 349.

[18] C.F. Baes, R.E. Mesmer, The Hydrolysis of Cations, John Wiley & Sons, New York, 1976, p. 292.

[18] H. Simillion, N. Van den Steen, H. Terryn, and J. Deconinck, Geometry influence on corrosion in dynamic thin film electrolytes, Electrochim. Acta, 209 (2016) 149.

[20] O. Dolgikh, H. Simillion, S.V. Lamaka, A.C. Bastos, Huibin B. Xue, M.G. Taryba, A.R. Oliveira, C.

Allély, B. Van Den Bossche K. Van Den Bergh J. Strycker, J. Deconinck Corrosion protection of steel cut-edges by hot-dip galvanized Al(Zn,Mg) coatings in 1 wt% NaCl: Part II. Numerical simulations, *Materials and Corrosion* 70 (2019) 780–792.

[21] M. M. Lohrengel, I. Klüppel, C. Rosenkranz, H. Bettermann, and J. W. Schultze, Electrochim. Acta 48 (2003) 3203.

[22] S. Van Damme, N. Smets, D. de Wilde, G. Weyns, and J. Deconinck, J. Phys. Chem. B 113 (2009) 3105.

APPENDIX 1 – Electrochemical methods used for obtaining the experimental data

This appendix provides a short description of the methods and techniques used for obtaining the experimental data shown in this work. It starts with the construction of the electrochemical cell, followed by the measurements of the galvanic current, potential of the galvanic couple, and polarization curves of zinc and iron. Then details are given about the measurements of potential in solution, ionic currents, dissolved O_2, pH, Zn^{2+}, Na^+ and Cl^-.

A1. Materials and electrochemical cell

Pure (99.9+%) zinc and iron wires with 1 mm diameter (Goodfellow, UK) were embedded in epoxy (Epokwick FC, Buheler, USA) mounts (cylinders with 1 cm height and 1.5 cm radius). Before each experiment, the surface of the mount was ground with SiC paper with grit sizes from 800 to 2500. The samples were finally rinsed with distilled water followed by ethanol. The metals were electrically connected from the other side of the mount. Adhesive tape applied around the epoxy holder provided the reservoir for the testing solutions (Figure 2). The Zn-Fe couple was immersed in NaCl solutions prepared with distilled water and NaCl of *pro analysis* quality. NaCl concentrations were 0.005 M, 0.05 M and 0.5 M NaCl.

A2. Galvanic current, potential of the galvanic couple, and polarization curves

The galvanic current flowing between the zinc and iron electrodes was measured with a zero-resistance ammeter (ZRA) using a PGStat 302N AUTOLAB potentiostat (Methrom AUTOLAB, The Netherlands) – Figure A1 a). The potential of the galvanic couple was measured against a saturated calomel electrode (SCE) – Figure A1 b). The results show noticeable differences in I_{galv} and E_{couple} when the couple is immersed in solutions of different NaCl concentration. The main effect seems to be the conductivity of the solution. The ohmic drop in solution increases for lower conductivities, leading to lower currents. The shift to more positive potentials seems to be due to the need of a higher overpotential to drive the required oxidation current.

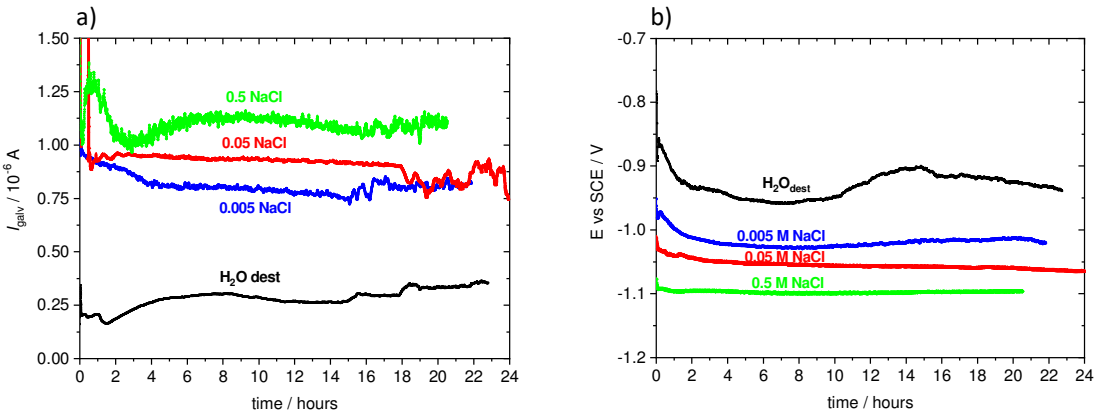

Figure A1 – a) galvanic current and b) galvanic potential of the Zn-iron couple immersed in distilled water and in 0.005, 0.05 and 0.5 M NaCl aqueous solution.

Polarization curves (linear sweep voltammograms) were acquired with the same potentiostat and the same electrochemical cell, in a 3-electrode configuration, with the individual Fe and Zn electrodes as working electrode, a platinum wire as counter electrode and a SCE as reference. Independent anodic and cathodic sweeps were recorded with a scan rate of 1 mV s^{-1} starting around the open circuit potential (OCP). Polarization curves measured after 1 hour and 1 day of immersion are presented in Figure A2. Differences indicate slight changes in the surface of the electrodes.

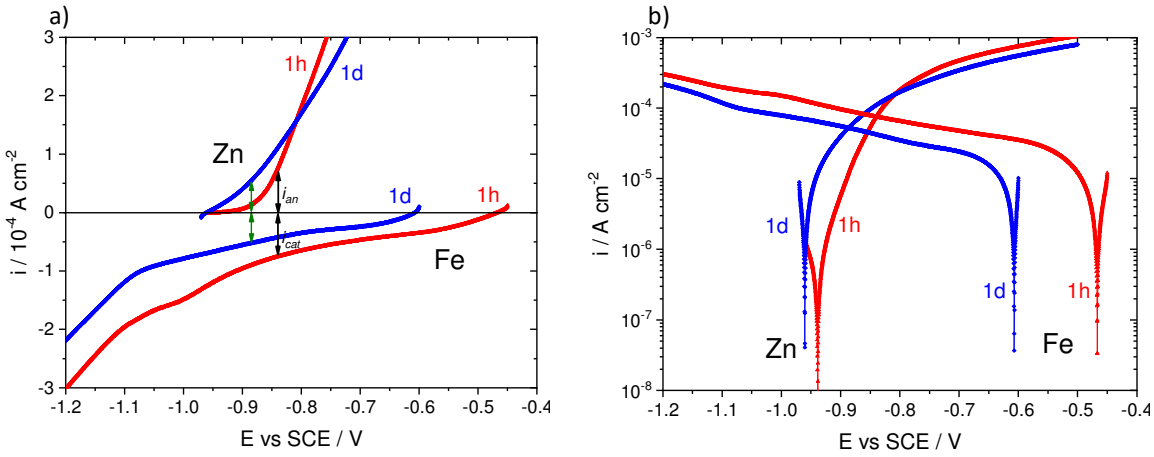

Figure A2 – Polarization curves of zinc and iron in 0.005 M NaCl (pH=5.7) after 1 hour and 1 day of immersion. In a) the current scale is linear and in b) the current is in logarithmic scale.

A3. Potential in solution

The distribution of potential in solution can be measured with a scanning micro-reference electrode with respect to another reference electrode placed in a fixed position in the cell. In this case a glass micropipette (2 µm in diameter) filled with 5mM NaCl and containing a Ag/AgCl wire was used as scanning microelectrode. The reference electrode was a homemade Ag/AgCl, 5 mM NaCl mini electrode with the inner solution stabilized by 3% agar-agar (see A6). The reference mini-electrode was fixed inside the cell, a few millimetres away from the galvanic couple. The electrodes were connected to a preamplifier used for micro-potentiometric measurements which scanned the solution in two planes, measuring maps of 50x50 points with a acquisition time of 0.2 s in each point.

A4. Current density in solution

The ionic currents in solution were measured with the Scanning Vibrating Electrode Technique (SVET) [A1]. This technique uses a vibrating microelectrode to sense the electric field in an electrolyte solution associated with the ionic currents flowing therein. When this is done close to a surface it is possible to identify the places where oxidation reactions occur (anodic regions) and where reductions take place (cathodic regions). In a typical SVET measurement, the vibrating microelectrode scans the surface (usually 50 to 200 µm above it) and measures the potential difference in solution, ΔV, between the ends of the vibration, Δr(10-40 µm are typical

values). The local current is given by,

$$i_{loc} = \frac{E}{\rho} = -\frac{1}{\rho}\frac{\Delta V}{\Delta r} \quad \text{(A1)}$$

where i_{loc} is the local current density, E is the electric field and ρ is the solution resistivity. In practice, instead of equation (A1) a calibration routine allows the system to immediately give the current density from the measured potential [A2]. The calibration is valid for a new solution provided the system is updated with its conductivity.

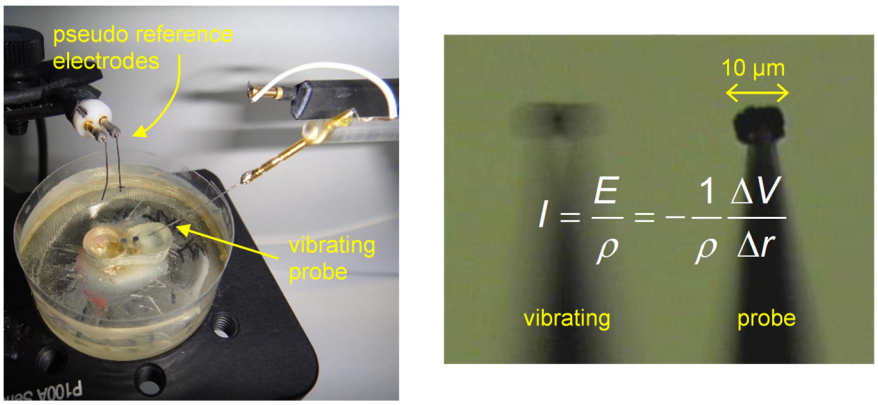

Figure A3 – Experimental setup for SVET measurements and details about the vibrating electrode.

The SVET equipment was manufactured by Applicable Electronics Inc. (USA) [A3] and controlled by the ASET 2.00 program developed by Sciencewares (USA) [A4]. The SVET microelectrode was prepared from polymer insulated platinum–iridium microelectrodes produced by Microprobes Inc. (USA) [A5]. A 20 µm diameter platinum black sphere was electrodeposited at the tip. The microelectrode vibrates in two directions, one parallel (x axis) and another normal (z axis) to the sample surface, sensing the electric field in the two directions. The x and z frequencies were 115 Hz and 69 Hz, respectively, and the amplitude of both vibrations was 10 µm. After arriving to a new point of measurement the probe waited 0.2 s and averaged for more 0.2 s before moving to the next point.

A5. Dissolved oxygen in solution measured by amperometric microelectrode

The measurement of dissolved oxygen was based on reaction (2),

$2H_2O(l) + O_2(g) + 4e^- \rightarrow 4OH^-(aq)$

and was performed with a IPA2 amplifier in the amperometric mode using a pre-amplifier for current detection, both produced by Applicable Electronics. This system uses two electrodes, a 10 µm diameter platinum microdisc (CH Instruments, USA, Ref. CHI100) as working electrode (sensor) and a homemade Ag|AgCl electrode as counter/reference electrode – Figure A4 a). Given the small currents to be measured (pico to nanoamperes) this electrode maintains its integrity and stable potential, despite being polarized. The tip potential was set at -0.7 V vs Ag|AgCl, well inside the oxygen diffusion control region – Figure A4 b). In this region the current magnitude only depends on the concentration of dissolved O_2. The measured tip current is

proportional to the concentration of dissolved oxygen in solution according to equation $I = 4\ n\ F\ D\ r\ C_{O2}$, where n is the number of electrons in the electrochemical reaction (4 in this case), F is the Faraday constant (96485 C mol^{-1}), D is the diffusion coefficient of O_2 (1.96 x 10^{-9} m^2 s^{-1}), r is the radius of the microelectrode tip (5 µm) and C_{O2} is the local concentration of dissolved O_2. Knowing I (which is the measured quantity) the local C_{O2} becomes available. The electrode and the pre-amplifier were mounted in the same 3D positioning system used for SVET and the measurements were controlled by the ASET software.

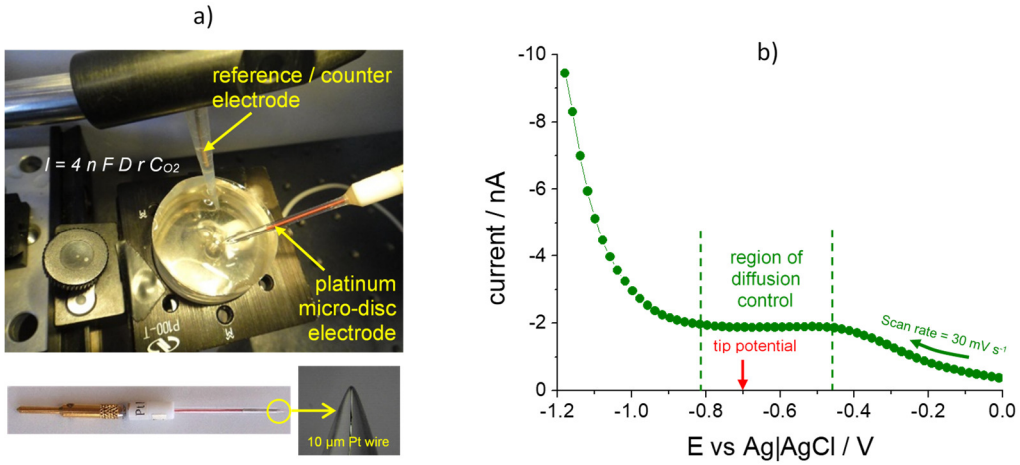

Figure A4 – a) Setup for the localised measurement of dissolved oxygen and b) voltammogram acquired with the Pt microelectrode, depicting the reduction of O_2 with the region of constant current due to the diffusion limitation and the potential at which the amperometric measurement was performed.

A6. Localized measurements of pH, Zn^{2+}, Na^+, Cl^- with potentiometric microelectrodes

Measurements of local concentrations of H^+/OH^- (pH), Zn^{2+}(aq), Na^+ and Cl^- were performed with homemade potentiometric microelectrodes – Figure A5 a). Borosilicate glass capillaries (WPI, USA, Ref. TW150-4) with 1.5 mm diameter were pulled with a P97 micropipette puller (Sutter, USA) to make micropipettes with a tip diameter of about 2 µm. The micropipettes were silanised for 2 hours in an oven at 200 ºC with 200 µL of N,N-dimethyltrimethylsilylamine (Fluka, Ref. 41716). The micropipettes was filled with an internal solution and an ionophore gel selective to each particular ion was inserted at the tip. The composition of the ionophore gel, the internal solution, and the length of the gel column at the microelectrode tip are presented in table A1. The micropipette was then inserted in a half-cell plastic holder (WPI, USA, Ref. EHB1) containing a silver|silver chloride wire as internal reference electrode. A homemade Ag|AgCl |0.005M NaCl electrode served as external reference electrode. The microelectrode was connected to a potentiometric pre-amplifier head (input resistance > 10^{15} Ω), which was mounted in the same 3D positioning system used for the other localised measurements. An IPA2 amplifier (input resistance > 10^{12} Ω) from Applicable Electronics was controlled by the ASET program (ScienceWares, USA) to measure and record the data. The local solution potential measurements referred in section A3 followed this set-up, except for the ion-selective membrane which was absent. The microelectrodes were calibrated with commercial pH buffers or standard solutions and the potentiometric response (calibration curves) is in Figure A5 b).

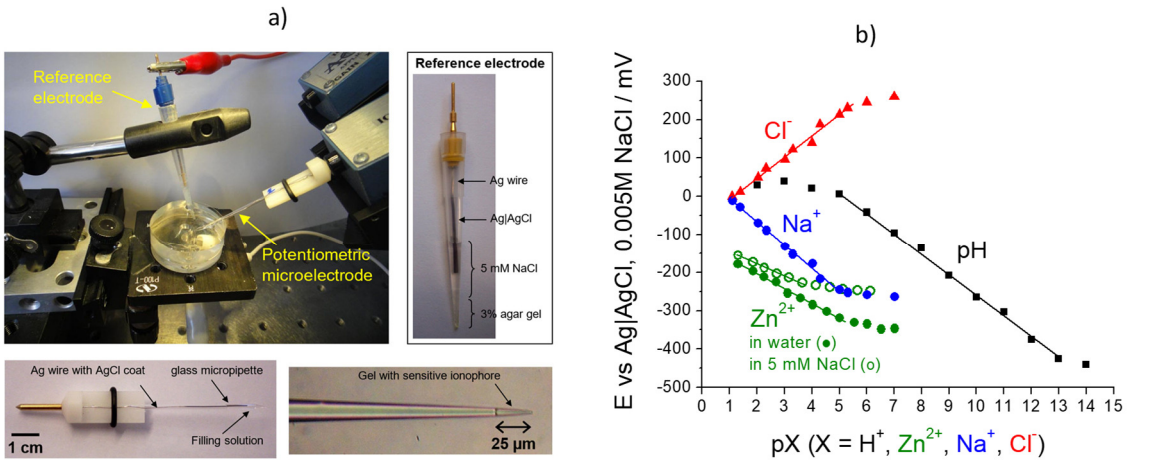

Figure A5 – a) Setup for the measurements with potentiometric microelectrodes with details about the electrodes used, b) calibration curves of the ion-selective microelectrodes for pH, Zn^{2+}, Cl^{-} and Na^{+}.

Table A1 – Composition of the ion-selective microelectrodes used

	Ionophore	Internal Solution	LIX column (µm)
pH	Hydrogen I cocktail B Fluka 95293	0.1M HCl + 0.01 M KH_2PO_4	25
Zn^{2+}	Tetra-n-butyl thiuram dissulfide based homemade cocktail	0.1M KCl + 0.01M KH_2PO_4 + 10^{-5}M $ZnCl_2$	70
Na^{+}	Sodium ionophore II cocktail A Fluka 71178	0.1M NaCl + 0.01M NaH_2PO_4	50
Cl^{-}	Chloride ionophore I cocktail A Fluka 24902	0.1M NaCl + 0.01M NaH_2PO_4	30

References

[A1] A.C. Bastos, M.C. Quevedo, O.V. Karavai, M.G.S. Ferreira, On the Application of the Scanning Vibrating Electrode Technique (SVET) to Corrosion Research, J. Electrochem. Soc. 164 (2017) C973.

[A2] L. F. Jaffe and R. Nuccitelli, "An ultrasensitive vibrating probe for measuring steady extracellular currents," J. Cell Biol., 63 (1974) 614; C. Scheffey, "Two approaches to construction of vibrating probes for electrical current measurement in solution," Rev. Sci. Instruments, 59 (1988) 787.

[A3] www.applicableelectronics.com (last view 15/June/2021).

[A4] www.sciencewares.com (last view 15/June/2021).

[A5] https://microprobes.com (last view 15/June/2021).